Biobased Composites from Eugenol- and Coumarin-Derived Methacrylic Latex and Hemp Nanocellulose: Cross-Linking via [2 + 2] Photocycloaddition and Barrier Properties

Sara Dalle Vacche, Samantha Molina-Gutiérrez, Giuseppe Ferraro, Vincent Ladmiral, Sylvain Caillol, Patrick Lacroix-Desmazes, Yves Leterrier, Roberta Bongiovanni

Biobased composites from eugenol- and coumarin-derived methacrylic latex and hemp nanocellulose: crosslinking via [2 + 2] photocycloaddition and barrier properties

Sara DALLE VACCHE [1,2], Samantha MOLINA-GUTIÉRREZ [1,3], Giuseppe FERRARO [1,], Vincent LADMIRAL [3], Sylvain CAILLOL [3], Patrick LACROIX-DESMAZES [3], Yves LETERRIER [4], Roberta BONGIOVANNI [1,2]*

[1] Dipartimento Scienza Applicata e tecnologia, Politecnico di Torino, c.so Duca degli Abruzzi 24, 10129 Torino, Italia

[2] INSTM-Politecnico di Torino Research Unit, 50121 Firenze, Italy

[3] ICGM, Univ Montpellier, ENSCM, CNRS, Montpellier, France

[4] Laboratory for Processing of Advanced Composites (LPAC), Ecole Polytechnique Fédérale de Lausanne (EPFL), CH-1015 Lausanne, Switzerland

KEYWORDS: Biobased composites, biobased latex, biomass filler, hemp nanocellulose, coumarin, cycloaddition, water vapor barrier.

ABSTRACT

A novel biobased latex was synthesized by redox initiated emulsion copolymerization of ethoxy dihydroeugenyl methacrylate with 5 wt.% of a photosensitive methacrylate containing a coumarin group. A stable copolymer latex having 16 wt.% solids content and a particle size of 53 nm was obtained. The copolymer had a Tg of 29 °C and was soluble in acetone. Coatings were obtained and the effect of UVA irradiation was tested: the light-induced crosslinking of the copolymer by [2 + 2] cycloaddition of the coumarin pendant moieties was demonstrated by UV-visible spectroscopy. As a consequence of UVA-induced crosslinking, the copolymer became insoluble in acetone. The copolymer latex was combined with hemp-derived nanocellulose to obtain composite self-standing films, by simple mixing in aqueous medium followed by casting, evaporation of water and hot pressing. The composite films were also successfully crosslinked by [2 + 2] cycloaddition, with an enhancement of barrier properties. The water vapor transmission rate of the crosslinked composite films with up to 45 wt% nanocellulose was 5 times lower than that of the hemp nanocellulose film, while further addition of nanocellulose increased permeability.

INTRODUCTION

The use of polymeric materials in several applications enhancing the quality and comfort of modern life has become widespread, although often at the cost of environmental damage and health hazards related to energy intensive and polluting production processes, exploitation of fossil resources, and incorrect waste disposal habits. The use of renewable resources, including upcycling of waste and valorization of biomass, the adoption of eco-friendly production

processes, and the design of new materials coupling durability with sustainable end-of-life options, are key strategies for solving these issues.

A great effort is ongoing to enlarge the platform of available biobased raw materials, including those derived from waste biomass through different refining and extraction processes. Cellulose, the most abundant natural polymer, can be extracted in the form of nanocellulose, i.e. nanofibrils or nanocrystals, from a wide variety of lignocellulosic biomasses, including, besides wood, abundant agricultural residues such as rice husks[1,2], corn stover[3,4] or hemp stems[5–7]. Nanocellulose shows in dry conditions remarkable mechanical and gas barrier properties, which are however dramatically affected in humid environments[8]. A well-recognized strategy to improve the water resistance of nanocellulose is to combine it with polymers[9]. Among polymeric materials, polymer networks, obtained via thermal or photoinduced crosslinking, offer distinct advantages, such as improved chemical resistance, absence of creep, and durability. Particularly, crosslinking processes induced by light exhibit remarkable energy efficiency and low volatile organic carbon emissions[10,11]; furthermore, the exploitation of renewable carbon[12,13] and the development of photoinitiator-free[14] or reversible[15] reactions are underway for further improving their safety and environmental friendliness.

Due to the polar nature of its molecular structure, rich in surface hydroxyl groups forming inter- and intra-molecular hydrogen bonds, nanocellulose tends to aggregate when mixed with non-polar monomers or oligomers[16]. Complex solvent mediated procedures or surface modification of nanocellulose were thus developed to improve dispersion and compatibility with non-polar polymers[17]. Waterborne polymer latexes offer a simple and environmentally convenient alternative as they can directly be mixed with nanocellulose in water suspensions. Synthesis of latexes from renewable resources has already been reported in the literature, but

mainly from vegetable oils, sugars or terpenes[18]. Although there have been some recent works on cardanol, vanillin, ferulic acid or eugenol derivatives[19–22] , including those of our team[23–25], the emulsion polymerization of biobased aromatic monomers remains underdeveloped, in particular the synthesis of aromatic copolymers.

An interesting option for imparting to polymer latexes the ability to form crosslinks is the introduction in the polymer structure of moieties able to dimerize upon irradiation with UV light, without the need for photoinitiators. Coumarin, a natural aromatic compound which can be extracted from several plants[26] dimerizes via a photochemical [2+2] cycloaddition. This reaction, known since the early 1900's[27], has in the last few decades been engineered in polymers to prepare light responsive networks[28]. Some works reported the photocrosslinking of polymer latex particles exploiting coumarin functional groups, introduced by copolymerization or post-polymerization functionalization[29,30]. Self-healing photo-responsive cellulose nanocrystal-modified fluorinated polyacrylates containing coumarin derivatives were synthesized by Pickering emulsion polymerization[31–33]. In addition, few examples of partially biobased photoresponsive polymer networks with coumarin functional groups have been reported[34,35]. However, to the best of our knowledge, coumarin-containing biobased polymer latexes photocrosslinkable via [2+2] photocycloaddition have not been widely investigated so far.

In previous work, we proposed the synthesis of a copolymer latex of ethoxy dihydroeugenyl methacrylate (EDMA) with 1 wt.% coumarin methacrylate (CouMA) by redox initiated emulsion polymerization; the latex was used to prepare composite films reinforced with wood-derived microfibrillated cellulose, whose oxygen permeability was investigated [36]. The introduction of coumarin moieties in the polymer backbone was found to decrease the oxygen permeability of the non-crosslinked composites, while only a slight further decrease was obtained by

crosslinking, possibly owing to low crosslink density. Extending this preliminary study, in the present work we synthesized an EDMA-based copolymer latex with a higher coumarin content, to allow for a higher crosslink density, performed its physico-chemical characterization and studied its crosslinking via [2+2] cycloaddition. We then prepared composite films with different weight fractions of hemp nanocellulose, prepared by our group to valorize an abundant local agricultural residue consisting of low-quality bast fibers separated from stalks discarded from plants harvested for oil and seeds[7]. We crosslinked the composites by exposure to UV light to produce insoluble materials, and we finally investigated the properties of the crosslinked composites, with particular focus on water vapor permeability.

EXPERIMENTAL SECTION

Materials. (4-methyl)coumarin-7-yl methacrylate (CouMA, Specific Polymers); ethylene carbonate (98%, Aldrich), 1,5- diazabicyclo[4.3.0]non-5-ene (DBN, 98%, Aldrich), methacrylic anhydride (94%, Aldrich), sodium dodecyl sulfate (SDS, >99%, Aldrich), potassium persulfate $K_2S_2O_8$, (KPS, ≥99.0%, Aldrich), sodium metabisulfite $Na_2S_2O_5$ (SMBS, 99%, Aldrich), sodium bicarbonate $NaHCO_3$ (99.7%, Aldrich), and dichloromethane (DCM, >99%, VWR) were used as received. Deionized water (DI water, 1 μS cm^{-1}) was obtained using a D8 ion exchange demineralizer from A2E Affinage de L'Eau. 2-(2-methoxy-4-propylphenoxy)ethyl methacrylate (Ethoxy Dihydroeugenyl MethAcrylate, EDMA) monomer was synthesized from dihydroeugenol (2-Methoxy-4-propylphenol, 98%, Aldrich) as described in previous work[37].

Emulsion copolymerization of EDMA with CouMA. The emulsion copolymerization of EDMA with CouMA (Scheme 1) was carried out in a 50 mL double-walled jacketed glass reactor with a U-shaped glass stirring rod, adapting the procedure previously published for the emulsion polymerization with redox initiation of EDMA monomer[38]; the recipe is summarized in

Table 1. The monomer mixture (5.86 g) was prepared by dissolving CouMA (5 wt.%) in EDMA; the mixture was purged under argon for 15 min, heating at 40 °C to allow for complete dissolution of CouMA. $K_2S_2O_8$ was dissolved in 9 mL of DI water and placed aside. SDS, $NaHCO_3$, $Na_2S_2O_5$ and the rest of the DI water (27.5 g) were mixed, placed in the reactor, and purged with argon for 30 min (Attention! $Na_2S_2O_5$ and $NaHCO_3$ will produce gas when mixed). The reactor was then heated to 40 °C and the mixture of monomers was added. Finally, 3 mL of the previously prepared solution of $K_2S_2O_8$ were added in one shot and this was considered as t = 0. The rest of the $K_2S_2O_8$ solution (6 mL) was added over four hours at 1.5 mL/h, and the polymerization proceeded under mechanical stirring at 200 rpm.

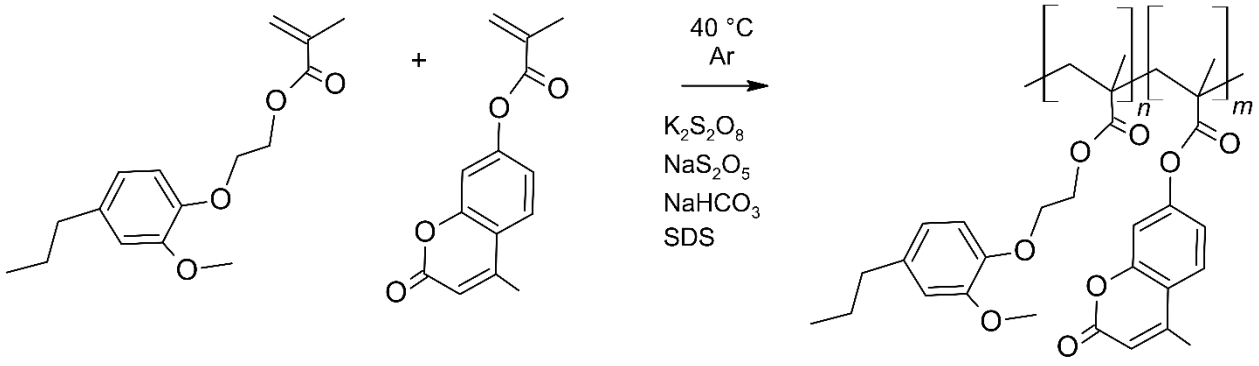

Scheme 1 Emulsion copolymerization of EDMA and CouMA

Table 1. Recipe for redox initiated emulsion copolymerization of EDMA and CouMA

Ingredient	**MW (g/mol)**	**Mass (g)**	**Equivalents**	**mmol**	**% wt** [1]
EDMA	278.35	5.5670	1.00	20.00	95.00
CouMA	244.25	0.2930	0.06	1.2	5.00
SDS	288.37	0.2344	0.041	0.81	
$K_2S_2O_8$	270.32	0.1172	0.022	0.43	
$Na_2S_2O_5$	190.11	0.1072	0.028	0.56	

$NaHCO_3$	84.00	0.1311	0.078	1.56
DI water		36.5493		

[1] % weight percent of monomers in the monomer mixture

Preparation of hemp nanocellulose and nanopaper. An aqueous suspension of hemp nanocellulose (1.3 wt.% solid content) was obtained from non-aligned bast fibers from hemp (*Cannabis sativa* L.) plants of the Carmagnola variety following a previously published procedure[7]. The suspension was formed by nanofibrils with lengths of 100 – 300 nm and widths of 5 – 12 nm, together with stacks of nanofibrils and larger micron sized fibers. A handsheet of hemp nanocellulose, indicated in what follows as hemp nanopaper (HNP), with a thickness of 53 μm, was prepared[7] between two precision woven nylon screening fabrics using a Rapid-Köthen standard sheet former (Frank-PTI, Germany) and was used as reference.

Preparation of poly(EDMA-*co*-CouMA) / hemp nanocellulose composite films. Hemp nanocellulose was diluted with demineralized water to a solids concentration of 1 wt.% by means of a T 10 ULTRA-TURRAX® homogenizer (IKA-Werke GmbH & Co. KG) at approximately 20k rpm. Then, the desired quantities of hemp nanocellulose suspension were added dropwise to the poly(EDMA-*co*-CouMA) latex while mixing using a magnetic stirrer for 10 minutes at 1000 rpm. The nanocellulose contents were 15 – 30 – 45 – 60 wt.% of nanocellulose (dry weight) with respect to total solids (dry nanocellulose + copolymer). After degassing under vacuum, the suspensions were cast on Petri dishes lined with a high-density polyethylene (HDPE) film and allowed to dry at ambient conditions until no weight change was detected. The films were then hot-pressed with a PEI LAB 150 P (Pinette Emidecau Industries) press at 80 °C with 2kN force for 10 min. Part of the composite films was crosslinked by exposure to UV light: a Dymax 2000-EC flood system equipped with a 400 W metal halide lamp (Dymax Corporation) with an emission spectrum in the UVA-UVB range[39] (wavelengths between 280 nm and 410 nm), was

used. The light intensity was fixed at 35 mW cm^{-2} during 20 min at a temperature of about 40 °C. The thicknesses of the obtained composite films ranged from 70 to 95 μm, and within a film the typical standard deviation for thickness was about 5μm.

Insoluble content. A sample of material of about 10 mg was weighed (m_i), wrapped in a metallic mesh and soaked at room temperature for 24 h in 10 mL of solvent (acetone or toluene). Then, after drying in an oven at 60 °C until a constant weight was reached, the final mass of the sample was recorded (m_f). The insoluble content (%) was calculated as $100 \cdot \frac{m_f}{m_i}$.

NMR spectroscopy was performed on poly(EDMA-*co*-CouMA) with a Bruker Avance 400 MHz spectrometer at room temperature. The spectra were recorded by dissolving 0.1 mL of sample in 0.5 mL of $CDCl_3$.:

1H NMR spectrum (400 MHz, $CDCl_3$, δ, ppm): 7.40 (m, 1H, **H**-Ar CouMA), 7.26 ($CHCl_3$),7.03 (m, 2H, **H**-Ar CouMA), 6.66 (m, 3H, $\mathbf{H_{5,3,6}}$-Ar), 6.18 (s,1H, **H**-Ar CouMA), 4.10 (m, 4H, OC$\mathbf{H_2}$C$\mathbf{H_2}$OPh), 3.78 (s, 3H, C$\mathbf{H_3}$OPh), 2.45 (t, 2H, $CH_3CH_2C\mathbf{H_2}$Ph), 2.31 ppm (s, 3H, C$\mathbf{H_3}$C=CH_2COO CouMA), 1.85 (m, 2H, OC=OC(CH_3)=C$\mathbf{H_2\alpha,\beta}$), 1.56 (m, 2H, $CH_3C\mathbf{H_2}CH_2$Ph), 0.97 (m, 6H, OC=OC(C$\mathbf{H_3}$)=CH_2α,β and C$\mathbf{H_3}CH_2CH_2$Ph).

Fourier Transform Infrared (FTIR) spectroscopy was performed in Attenuated Total Reflectance (ATR) mode with a Nicolet iS50 spectrometer (Thermo Fisher Scientific Inc) fitted with an ATR-Smart Orbit accessory with a diamond crystal. The spectra were taken in the 550 – 4000 cm^{-1} range, with 32 scans per spectrum and a resolution of 4 cm^{-1}.

Dynamic Light Scattering (DLS). A Vasco 3 nanoparticle size analyzer (Cordouan Technologies) was used for performing particle size measurements on the latex by dynamic light scattering using the Cumulant model, at a temperature of 25 °C. The laser power, time interval,

and number of channels were adjusted to obtain a good autocorrelation function (ACF). Samples for DLS measurements were prepared by diluting one drop of latex with 5 mL of DI water, and the results are the average of 6 measurements.

UV-Visible spectroscopy. UV-Visible spectroscopy was performed by means of a JENWAY 6850 UV/Vis (Cole-Parmer, UK) UV-visible spectrophotometer in transmission mode. To avoid saturation of the signal, polymer and composite layers, having thickness of about 10-20 μm to avoid saturation of the signal, were coated on the side of a quartz cuvette as explained in what follows. The poly(EDMA-*co*-CouMA) latex was dried in an oven at 80 °C and then dissolved in acetone at a 1.5 wt.% concentration. A drop of the acetone solution was cast onto the side of a quartz cuvette, and acetone was evaporated in an oven at 40 °C prior to the analysis. Also, composite samples with 15 wt.% cellulose were analyzed: the nanocellulose containing latex suspension was further diluted with demineralized water, then a drop was cast on the side of the cuvette and dried at 80 °C to obtain a composite thin coating. To this aim, the samples were irradiated with UV light using a high-pressure mercury-xenon lamp Lightning Cure LC8 model L9588-02A[40], equipped with a flexible light guide and optional optical filters, A9616-07 or A9616-11, allowing selecting a specific wavelength range (Hamamatsu Photonics K.K.). To induce the photodimerization of coumarin moieties, favored at wavelengths longer than 300 nm, irradiation was performed either using a A9616-07 filter with a transmittance wavelength 355-375 nm (λ_{max} = 365 nm, UVA_{365}) or through a polyethylene terephthalate (PET) foil transmitting light above 307 nm (UVA and UVB). To assess the capability of coumarin dimers to revert to their original form, after achieving photodimerization by UVA_{365} light irradiation, the coatings were further irradiated with UVC light using an A9616-11 filter with a transmittance wavelength 230-250 nm (λ_{max} = 248 nm, UVC). The LC8 lamp and the filters were manufactured by

Hamamatsu. An EIT Powerpuck® II radiometer was used to measure the light intensity that was fixed at 36 mW cm^{-2} for UVA irradiation and at 7 mW cm^{-2} for UVC irradiation. UV-vis spectra were taken after irradiating the samples for given time intervals. The intensity of the absorbance at 318 nm was monitored to assess the extent of the photoreactions.

Differential scanning calorimetry (DSC) was carried out by means of a a Netzsch DSC 204 F1 Phoenix at a heating/cooling rate of 20 °C min^{-1} under N_2 flux. The temperature range was from -70 °C to 150 °C for the neat copolymer, and -70°C to 200°C for the composites. A heat–cool– heat procedure was performed (with two cooling/heating cycles for the polymers and three cooling/heating cycles for the composites), and the glass transition temperature (T_g) was taken at the inflection point of the glass transition step in the last heating cycle. The data obtained was processed with Netzsch Proteus Analysis software.

Thermogravimetric analysis with evolved gas analysis (TGA-FTIR) was performed using a NETZSCH TG 209 F1 Libra, increasing the temperature from 25 °C to 800 °C with a heating rate of 20 °C min^{-1}, under a 20 mL min^{-1} N_2 flux, to prevent thermo-oxidative processes. The first derivative of the residual mass curve (DTG) was calculated to better resolve the main thermal decomposition steps of the analyzed materials with Netzsch Proteus Analysis software. For evolved gas analysis the TGA was coupled to a Bruker Optics GmbH Tensor II gas IR module.

Scanning Electron Microscopy. Images of the surfaces and freeze-fractured cross-sections of the composite films were taken using a ZEISS SUPRA 40 Field Emission Scanning Electron Microscope (FESEM) equipped with a Gemini column (Carl Zeiss S.p.A.), with an acceleration voltage of 3 or 5 kV. Prior imaging, the samples were coated with platinum to prevent charging.

Wettability. The wettability of the films was investigated by static contact angle measurements performed at room temperature by means of an FTA 1000C instrument (First Ten Ångstroms, Inc.) equipped with a video camera and image analyzer, using the sessile drop technique. The probe liquids were water (5 μl drop) and hexadecane (3 μl drop). Several measurements per liquid were performed on each sample placing the drops in different parts of the sample surface.

Water vapor transmission rate (WVTR). The water vapor permeability of the crosslinked composite films was assessed by means of a PERMATRAN W 3/33 analyzer (Mocon) having a resolution of 0.0001 g m^{-2} day^{-1}. The hemp nanopaper and a composite film with 30 wt.% nanocellulose that was not subjected to crosslinking were also analyzed in the same way for reference. The measurements were performed according to the ASTM F1249-13 standard, and the test conditions were 38 °C ± 1 °C and 50 ± 3% or 90 ± 3% relative humidity (RH). Prior to test, following the ISO 291 standard, the materials were stored at 23 ± 1 °C, 50 ± 2% RH during at least 48 h. The carrier gas was dry nitrogen with a flow of 10 mL min^{-1} and the exposed sample surface was reduced to 1 cm^2 using aluminum masks: with these conditions the instrument's measuring range for WVTR is from 0.25 to 500 g m^{-2} day^{-1}. The instantaneous WVTR value was recorded as a function of time; once a steady state was obtained, the WVTR of each material was calculated as the average of the values recorded during 8 – 10 hours. Namely, when the RH was set to 50 %, the WVTR was taken as the average of the values between the 40^{th} and 48^{th} hour of analysis for samples with nanocellulose contents up to 45 wt.%, and between the 68^{th} and 78^{th} hour of analysis for samples with 60 wt.% nanocellulose and for the nanopaper. When the RH was set to 90 %, the average WVTR was taken between the 106^{th} and

116th hour of analysis. The WVTR values were then normalized to a thickness of 100 µm ($WVTR_{100}$) according to equation (3), where ℓ is the thickness in µm of the tested sample:

$$WVTR_{100} = \frac{WVTR \cdot \ell}{100} \quad (3)$$

RESULTS AND DISCUSSION

Synthesis and characterization of Poly(EDMA-*co*-CouMA) latex. The copolymerization process followed was inspired by previous experiments executed by the team[36,38] . As previous work showed that double bonds present on the side chain of eugenol derivatives lead to undesired premature crosslinking[38], the monomer ethoxy dihydroeugenyl methacrylate (EDMA), which has no unsaturation on the alkyl chain, was chosen among eugenol derivatives for the copolymerization with the photosensitive comonomer coumarin methacrylate (CouMA). The weight ratio of EDMA to CouMA was set to 95 : 5; weight ratios of CouMA higher than 5 wt% could not successfully be solubilized in EDMA at 40 °C. Both eugenol and 7-hydroxy-4-methylcoumarin, the precursors of our methacrylated monomers, are natural molecules[41,42]. The biobased contents of EDMA and CouMA, accounting for the methacrylation of the natural compounds with non-biobased chemicals, are 63 wt% and 71 wt%, respectively. With the set 95 : 5 monomer weight ratio, the resulting biobased content of the copolymer is about 63 wt.% (see calculation in Table S1). Emulsion polymerization was chosen as the technique to synthesize the polymer due to the sustainability benefits that it could bring to the latex in terms of water as an innocuous continuous phase (no contribution to VOC in the mixture). Using a redox initiation system at a temperature of 40 °C allowed the use of significantly lower energy in comparison to

thermal initiation: for most pure acrylates a conventional latex synthesis is carried out under thermal initiation at 75 – 90°C.

The emulsion polymerization of EDMA and CouMA yielded a stable latex of poly(EDMA-*co*-CouMA) at 16 wt.% solids content, with a diameter of 53 nm (D_i, intensity-average particle diameter measured by DLS). With the set 5 wt.% content of CouMA in the monomer mixture, the expected average molar ratio of EDMA to CouMA moieties in the copolymer (n : m) is about 17 : 1. From the 1H-NMR spectra the copolymer structure was confirmed (see Experimental section and NMR spectrum in SI, Figure S1), as well as the molar ratio of monomers. Moreover, the methacrylic hydrogens (δ = 5.57 ppm and 6.13 ppm) were absent.

The FTIR spectra of poly(EDMA-co-CouMA), and of poly(EDMA) reported as reference, are shown in Figure 1.

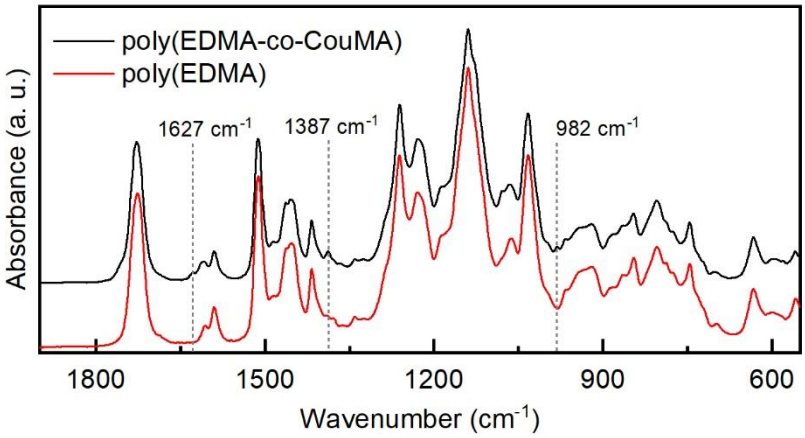

Figure 1 FTIR spectra taken in ATR mode of poly(EDMA-*co*-CouMA) and of poly(EDMA), characteristic signals of CouMA are indicated by dashed lines.

A strong absorption signal was present for both polymers at 1726 cm^{-1} for the stretching of the C=O bonds on the methacrylic backbone; the carbonyl group of coumarin, absorbing at slightly

higher wavenumbers, around 1760 cm^{-1}, was visible as a shoulder only for poly(EDMA-*co*-CouMA). Other absorptions characteristic of the coumarin molecule were relatively weak, due to the low amount of CouMA units in the copolymer: they were present at 1627 cm^{-1} for C=C stretching in the 3,4 position, 1387 cm^{-1} and 980 cm^{-1} for bending and rocking, respectively, of C-H in the 2-pyrone structure[43].

The latex was dried at 40 °C to prepare copolymer films for characterization. However, self-standing films suitable for mechanical and permeability characterization could not be obtained: the copolymer films cracked upon drying or when detached from the substrate**.** The copolymer was completely soluble in acetone demonstrating the lack of any significant crosslinking that would lead to the presence of an insoluble fraction (gel content).

The T_g of the copolymer, measured by DSC, was 29 °C, thus slightly higher than the T_g of 25 °C previously found for the homopolymer poly(EDMA), as shown in Figure S2. The introduction of the coumarin derivative in the polymer chain also slightly increased thermal stability, assessed by TGA in N_2 atmosphere (Figure 2): the $T_{d20\%}$ was 347 °C for poly(EDMA-*co*-CouMA) while it was 334 °C for poly(EDMA); from the DTG (first derivative of the residual mass curve) a main mass loss event was identified with T_{max} = 375 °C for both polymers. The FTIR analysis performed on of the evolved volatile products (Figure S3) for poly(EDMA-*co*-CouMA) at T_{max} showed signals in the 3100 – 2700 cm^{-1} for hydrocarbons, 1800 – 1660 cm^{-1} for carbonyl functional groups, and distinct signals at 1630, 1609 and 1183 cm^{-1} characteristic of the aromatic and 2-pyrone structures, confirming that this corresponded to the thermal decomposition of the polymer chain. A smaller decomposition event was present above 750 °C where the FTIR spectra of the evolved gas showed the most intense bands in the 2400 – 2000 cm^{-1} range for CO_2 and CO.

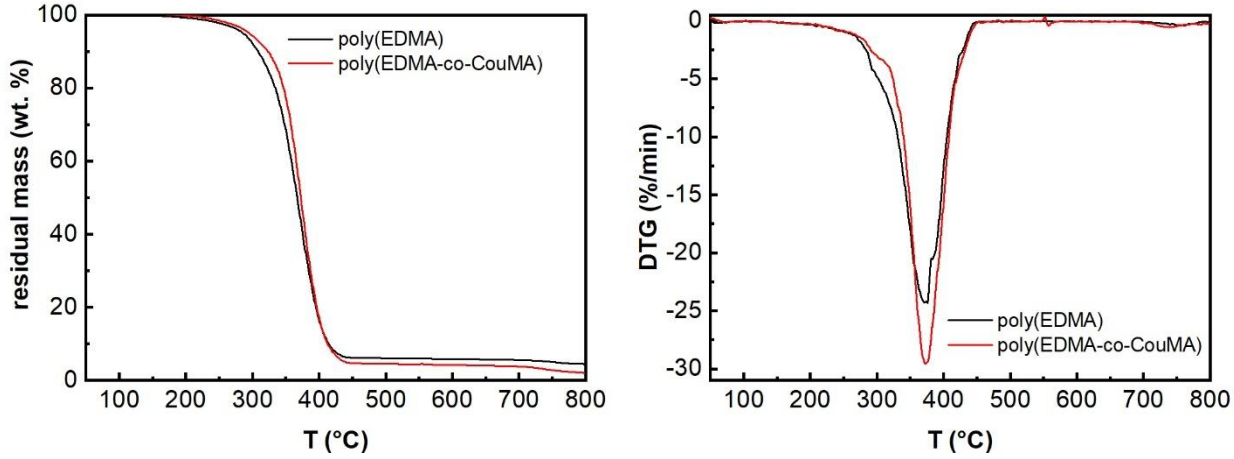

Figure 2 Thermogravimetric analysis of poly(EDMA-*co*-CouMA) compared to poly(EDMA): residual mass versus temperature curves and their first derivative (DTG).

Crosslinking of poly(EDMA-*co*-CouMA) via [2+2] photocycloaddition. Coatings cast on the side of quartz cuvettes as explained in the experimental section were irradiated with UVA light to induce crosslinking through [2 + 2] photocycloaddition of the coumarin moieties, as depicted in Scheme 2.

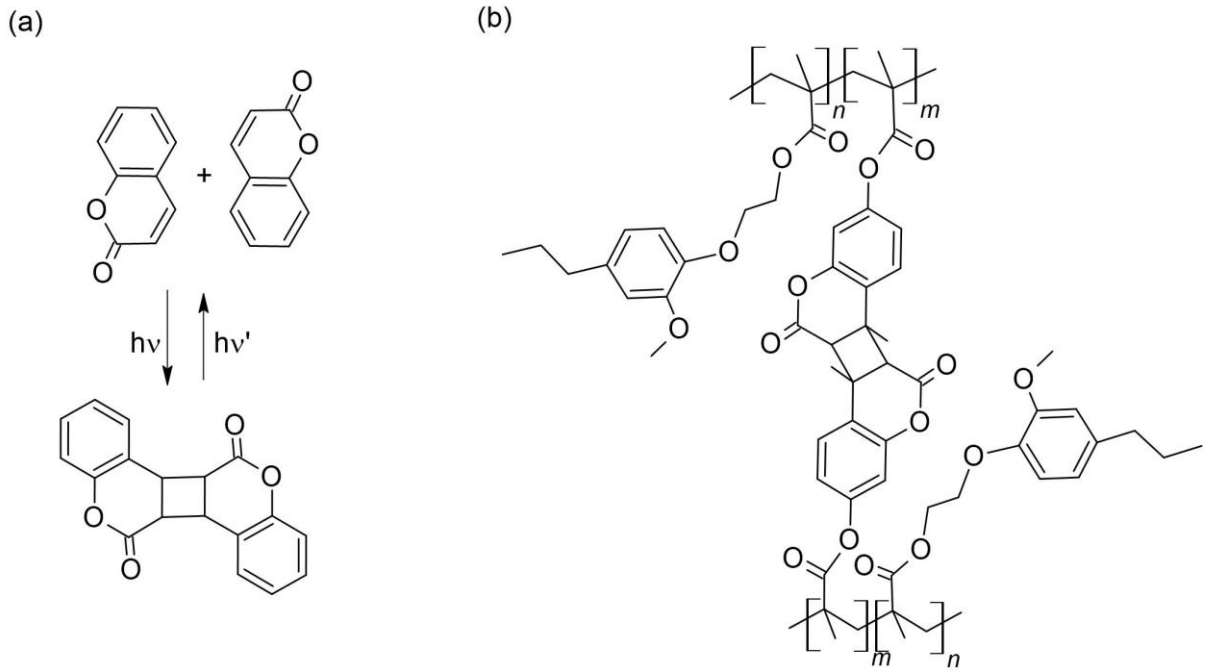

Scheme 2 (a) [2 + 2] photocycloaddition of coumarins; (b) poly(EDMA)-*co*-CouMA crosslinked via [2 + 2] photocycloaddition

The advancement of the crosslinking reaction was followed by UV-visible spectroscopy. The UV-visible spectrum of pristine poly(EDMA-*co*-CouMA) reported in **Figure 3** (spectrum at 0 min of irradiation) showed two broad absorption bands in the 250 – 380 nm region. The band above 300 nm, centered at about 318 nm, absent in the spectrum of poly(EDMA) (Figure S4), is characteristic of the 2-pyrone structure of coumarins, while the band below 300 nm, centered at about 280 nm, is characteristic of π–π^* transitions of the aromatic structures present in both the CouMA and EDMA moieties[44,45]. The decrease of the intensity of the signal at 318 nm during irradiation with UVA reflects the opening of the 3,4 double bond in the 2-pyrone structure to form the cyclobutane ring when coumarin dimers are formed[45,46]. The photocycloaddition of the coumarin pendant moieties proceeded during irradiation with UVA. When light at 355 – 375 nm (λ_{max} = 365 nm, UVA_{365}) was used, the coumarin double bond reached an almost complete conversion within 180 min (Figure 3a). The possibility to increase the crosslinking reaction rate by irradiation in a wavelength range closer to the absorption maximum of CouMA (318 nm) was also checked: when polychromatic light above 310 nm was used, the conversion was complete already after 20 min (Figure S4).

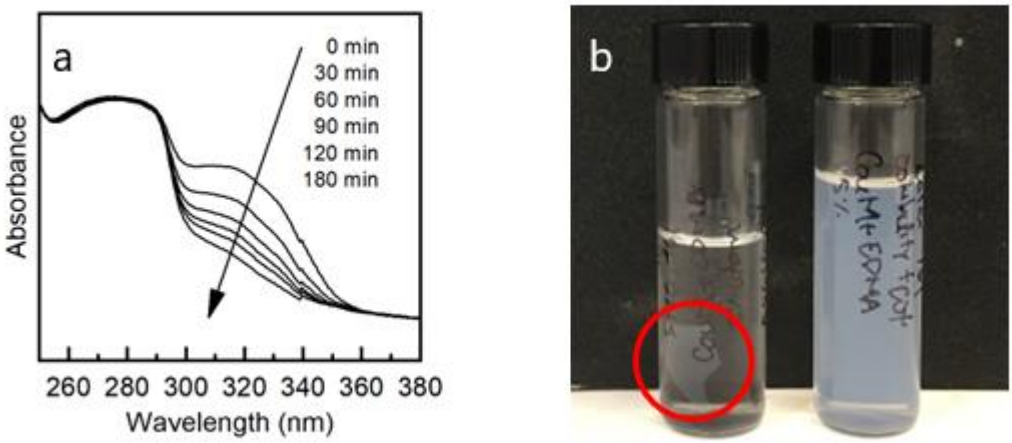

Figure 3. (a) UV-visible spectra of poly(EDMA-*co*-CouMA) latex irradiated with UVA_{365} light with a 36 mW cm^2 intensity for up to 180 min; (b) non-irradiated (right side) and UVA_{365}-irradiated (left side) poly(EDMA-co-CouMA) latex films after immersion in acetone: the non-irradiated film was completely soluble while the UVA_{365}-irradiated film remained insoluble as shown in the red circle.

To assess the possibility to obtain reversion of the [2+2] photocycloaddition reaction, latex coatings previously crosslinked via UVA_{365} irradiation were exposed to UVC light (λ_{max} = 248 nm, intensity of 7 mW cm^{-1}). Reversion to the pristine coumarin form was very limited and only detected up to 30 s of UVC irradiation, slightly increasing when the previous irradiation with UVA_{365} had been performed for a relatively short time, e.g. 20 min, thus not reaching complete conversion of CouMA moieties to the dimer form (**Figure 4**). Continuing the irradiation with UVC for longer times, a degradation phenomenon, also observed for UVC-irradiated poly(EDMA), appeared as indicated by the changes in the UV-vis absorption spectra shown in Figure S4. Indeed, irradiation at 254 nm or shorter wavelengths was reported to lead to photodegradation of polymethacrylate backbones[47].

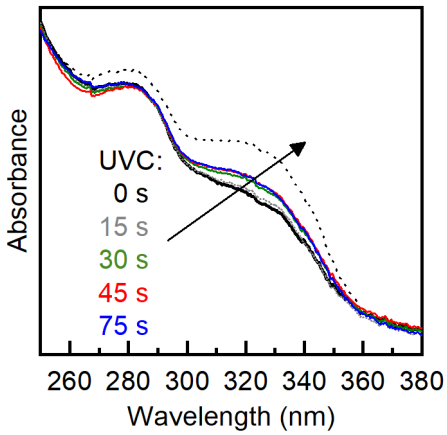

Figure 4. UV-vis spectra of poly(EDMA-*co*-CouMA) film irradiated first with UVA_{365} light with a 36 mW cm^{-2} intensity for 20 min (thick black line) and then with UVC light at 7 mW cm^2 intensity for up to 75 s. The spectrum of the non-irradiated latex film is reported as reference (dotted line).

After crosslinking with UVA_{365}, visually, the copolymer films developed a yellowish color, that can be attributed to the formation of coumarin dimers[48,49]. Notably, crosslinking dramatically affected the solubility of the copolymer (as also qualitatively shown in Figure 3b): while the non-irradiated copolymer sample was completely dissolved in acetone (insoluble content was 1-3 wt.%), the insoluble content of the copolymer exposed to UVA_{365} irradiation at 36 mW/cm^2 for 20 min was already 75 wt.% while after 180 min of exposure it was found to be 93 wt.%, confirming an efficient crosslinking. On the contrary, the same irradiation treatment did not affect the solubility of the homopolymer poly(EDMA), which was completely soluble in acetone both before and after irradiation.

From DSC analysis, irradiation of the copolymer with UVA_{365} for 180 min resulted in a slight broadening of the glass transition region, with a modest increase of T_g from 29 °C before irradiation to 33 °C after irradiation (see Figure S2). This may indicate that the network formed was quite loose, as expected: in fact, a 5 wt% content of coumarin moieties corresponds to 1

CouMA unit every 17 EDMA units, from which a maximum crosslink density of 10^{-4} mol cm^{-3} may be obtained.

A comparison of the thermogravimetric analysis results obtained for the non-irradiated and the irradiated copolymer (Figure S5) showed only minor differences, such as the shift at slightly higher temperature of the small decomposition event present above 750 °C.

[2+2] photocycloaddition in the presence of hemp nanocellulose. The copolymer latex was mixed with hemp nanocellulose to obtain composite materials: FESEM images of the nanocellulose are shown in Figure S7. To monitor the dimerization of the copolymer's CouMA moieties in the presence of the nanocellulose filler, composite coatings, obtained by casting a drop of diluted latex-nanocellulose suspension on quartz slides, followed by drying, were subjected to irradiation with UVA_{365} light. The UV-visible spectra were recorded with increasing irradiation times: in **Figure 5** the spectra recorded for the composite with 15 wt.% nanocellulose are reported. The dimerization proceeded to high conversion, within similar times as for the filler-free copolymer.

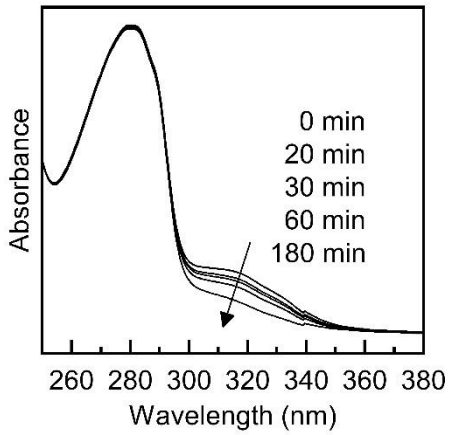

Figure 5. UV-visible spectra of coatings of poly(EDMA-*co*-CouMA) containing 15 wt.% of hemp nanocellulose, irradiated with UVA_{365} light for different times.

Characterization of composite films. Composite films with cellulose contents ranging from 15 to 60 wt.% (Figure 6) were prepared by simply mixing the latex with the diluted aqueous nanocellulose suspension, casting and drying in an oven at 40 °C followed by hot pressing at 80 °C. As the cellulosic filler was 100% biobased, the composites had a high biobased content, ranging from 69 wt.% to 85 wt.% (calculation in SI, Table S2). The films were self-standing but fragile, particularly at the low nanocellulose contents. They were transparent, with a brownish color imparted by the hemp nanocellulose. The colorimetric evaluation of the films is reported in Table S3.

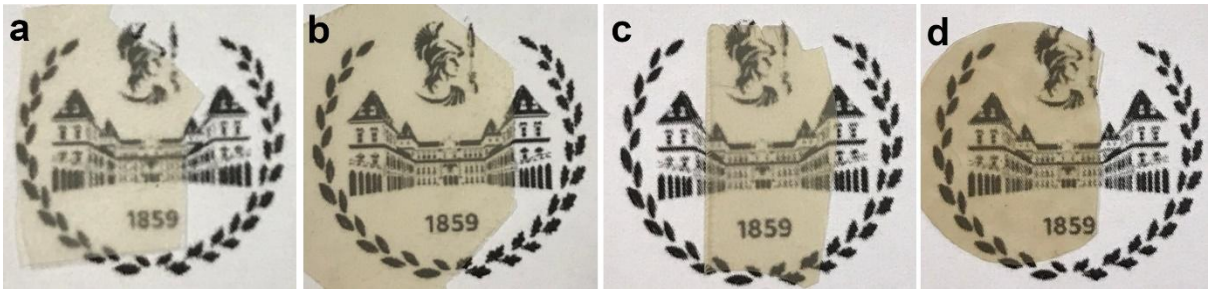

Figure 6. Photos of composites with weight fractions of hemp nanocellulose equal to: (a) 15 wt.%; (b) 30 wt.%; (c) 45 wt.%; (d) 60 wt.%.

When the films were irradiated with UV light as described in the experimental section to achieve crosslinking, the irradiation caused a yellowing of the composites (see Table S3), reflecting the observed yellowing of the copolymer matrix. The crosslinked composites were completely insoluble in acetone and in toluene (insoluble content ≥ 99 wt.%). As nanocellulose is insoluble in acetone, an increase of the insoluble fraction proportional to the cellulose weight fraction is expected for the crosslinked composites with respect to the unfilled crosslinked copolymer. Being the insoluble content of the crosslinked copolymer around 93 wt.%, and the cellulose content of the composites in the 15 wt.% to 60 wt.% range, insoluble fractions are

expected to be between 94% and 97%. However, nanocellulose may physically interact in several ways with the polymer chains and with the solvent: the fibrils network can either make the polymer less accessible to the solvent or retain the polymer chains through secondary interactions. As a consequence, there is a few percents increase of the insoluble content with respect to the expected value.

The surface of both the non-crosslinked and crosslinked composites, observed by FESEM, reflected the morphology of the nanocellulose (Figure S7): fibrils and stacks of fibrils of different dimensions were visible. Comparing the micrographs of non-crosslinked and crosslinked composites, a surface morphology change is evident, possibly due to combined effect of shrinkage of the matrix [50] and of microdefect healing upon photodimerization[51]. The observation of freeze-fractured cross-sections of crosslinked composites with 15 wt.% and 60 wt.% nanocellulose showed that the composites with the highest nanocellulose content had larger porosity (Figure S8).

The strongest effect of irradiation on composite films was the change in water vapor barrier properties. Measurements of water vapor transmission rate (WVTR) were performed on composites before and after crosslinking, at 38 °C and two different relative humidity (RH) conditions, i.e. 50 % and 90 %. The WVTR of filler-free copolymer films could not be assessed, as defect free self-standing films suitable for permeability measurements could not be obtained. The WVTR of the hemp nanopaper at 38 °C and 50% RH was measured and taken as reference: the value of 167 g m^{-2} day^{-1} measured for the 53 μm-thick handsheet, (corresponding to a $WVTR_{100}$ of 89 g m^{-2} day^{-1}) is in the range reported for MFC films[52]. Indeed, while common paper, obtained from larger cellulose fibers, is highly permeable to water vapor, nanocellulose sheets show, at low RH% conditions (RH<50%), moderate to low permeability to water vapor,

owing to the formation of a tight fibril network through hydrogen bonds, which is however disrupted at high RH%[53]. When measurements were performed on composite films before crosslinking, already at 50 % RH their permeability was so high that the WVTR was above the measuring range of the instrument, i.e. 500 g m^{-2} day^{-1}. The barrier properties towards water vapor of the non-crosslinked composites were thus much worse than those of reference nanopaper, possibly owing to the presence of submicrometric pinholes (as shown in Figure S7), and measurements at higher RH, where even higher permeability is expected, were not attempted. In contrast, the WVTR of the crosslinked composites was in all cases measurable, clearly indicating positive effect of crosslinking on barrier properties, consistent with the observed microdefect healing. The results obtained for crosslinked composites are summarized in Table 2, where for easier comparison all WVTR values are normalized to a thickness of 100 μm ($WVTR_{100}$) according to eq. 3.

Table 2 Water vapor transmission rates normalized to a thickness of 100 μm ($WVTR_{100}$) of crosslinked composites and hemp nanopaper.

Nanocellulose (wt.%)	**$WVTR_{100}$ @ 38 °C 50 % RH** ($g\ m^{-2}\ day^{-1}$)	**$WVTR_{100}$ @38 °C 90 % RH** ($g\ m^{-2}\ day^{-1}$)
15	18	274
30	22	-
45	15	350
60	117	-
100 (hemp nanopaper)	89	-

The $WVTR_{100}$ values of the crosslinked films containing up to 45 wt.% of cellulose were in the 15 – 22 g m^{-2} day^{-1} range, therefore lower than that of the hemp nanopaper taken as reference,

i.e. 89 g m^{-2} day^{-1}. The $WVTR_{100}$ increased to 117, above the value measured for hemp nanopaper, when the cellulose content was 60 wt.%: this abrupt increase may be ascribed to interfacial defects or filler agglomeration appearing at high filler contents. Permeation of water vapor across nanocellulose sheets happens through diffusion in the defective amorphous regions of the fibrils and within the porous structure formed by the fibrils network[53,54]. Our hemp nanocellulose fibrils, as reported in our previous study[7], have a high degree of crystallinity, thus are mostly impermeable to water vapor. When nanocellulose is dispersed in the polymeric matrix, permeation of the water molecules takes place through the polymer as well as in the interface regions between polymer and fibrils. The presence of well dispersed fibrils, as typically achieved at lower cellulose contents, imparts tortuosity to the gas path, decreasing permeability; on the other hand, at high nanocellulose contents, aggregates of fibrils or high matrix-fibril interfacial area, where defects may act as preferential paths for permeation, increase permeability.

When the RH was increased to 90 %, the $WVTR_{100}$, measured for the crosslinked composites containing 15 wt.% and 45 wt.% of nanocellulose, became 15 times and 22 times higher, respectively. Thus, a larger impact of RH on the permeability was confirmed for higher cellulose contents. Notice that this high sensitivity of WVTR to moisture is comparable to what was reported for nanocellulose/PLA composites[55], and lower than what was found in the case of nanocellulose films[56,57]. The $WVTR_{100}$ values obtained at 50% RH for the films with cellulose contents up to 45 wt.% were lower than those reported for other barrier films obtained combining microfibrillated cellulose (MFC) with other polymers, such as starch or beeswax coated MFC [58] or composites with photocured PEGDA or soybean oil epoxidized acrylate with comparable MFC contents[59]; furthermore the $WVTR_{100}$ measured at 90 % RH, although higher than those

reported for PLA and PCL [60], were lower than for e.g. cellulose acetate or cellulose acetate propionate[61].

The contact angles of water and hexadecane were measured on the two faces of the composites, and on the hemp nanopaper taken as a reference (Figure 7).

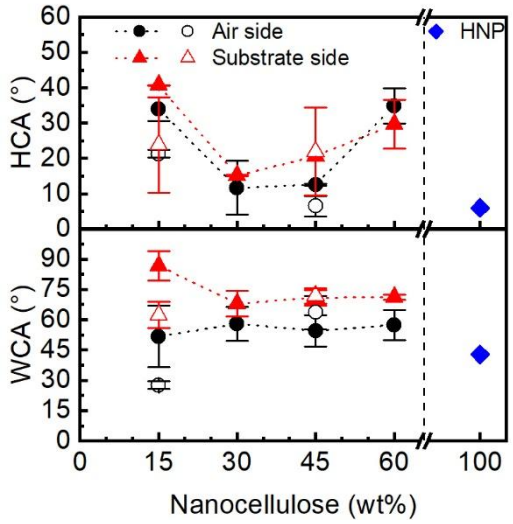

Figure 7. Water (WCA) and hexadecane (HCA) contact angles on air side and mold side for poly(EDMA-*co*-CouMA) based composites and for hemp nanopaper (HNP). Full symbols are for non-crosslinked composites and hollow symbols for crosslinked composites.

The water and hexadecane contact angle for the hemp nanopaper were low, as expected, being 43° and 6°, respectively; for each test liquid similar values were measured on both sides of the film as expected, as the nanopaper was manufactured between two identical nylon cloths. The surface energy was estimated as 57 mN m^{-1}, which is in line with other values reported in literature for nanocellulose films[62]. The wettabilities of the composites, both before and after irradiation, were affected by the presence of the non-polar polymer, as well as by that of the SDS surfactant. Notably, the composites were cast on a HDPE-lined open mold, thus one side of the film was exposed to air during drying (air side) and the other side was in contact with HDPE

(substrate side): different values for the WCA were obtained for the air side and the substrate side of the composite films, indicating a preferential arrangement of the components towards one of the sides. On the air side the contact angle of water was similar for all composites, in the 52 - 58° range, while on the substrate side it decreased from 86° for the 15 wt.% composite to around 70° for the other composites. For composite with 15 wt.% nanocellulose the variability of the contact angle was larger on the air side (standard deviation of 15°) than on the substrate side (standard deviation of 7°). This large variability was attributed mainly to an inhomogeneous presence of the SDS surfactant at the surface, as confirmed by infrared spectroscopic analysis: characteristic bands of SDS [63,64] i.e. CH_2 asymmetric and symmetric stretching at 2916 cm^{-1} and 2849 cm^{-1}, respectively, and S-O asymmetric and symmetric stretching at 1220 cm^{-1} and 1080 cm^{-1}, respectively, are very evident in the FTIR spectrum of the air side of the composite film (cfr. Figure S9). Surfactants preferentially migrate to the interfaces between substances of very different polarities: in the case of these composites the interfaces are between the nanocellulose and the polymer and the surface of the film towards air. When nanocellulose concentration is low, the interfacial area between microfibrils and polymer is smaller, thus a larger amount of surfactant is free to migrate to the surface where it can segregate, forming islands. Indeed the 15 wt.% composite showed a larger difference between the WCA on the air side and that on the substrate side than the other composites. Hexadecane contact angles for the composites were always larger than for the nanopaper and had larger values for the lowest and highest nanocellulose concentrations, on both sides of the composite films.

The thermal analysis of the composites performed by DSC (Figure S2) showed glass transition in the same temperature region as for the unfilled copolymer and, in the first heating cycle only,

the characteristic endothermic broad peak corresponding to evaporation of residual water. No other transitions were detected.

Thermogravimetric analyses were performed on the composites, and on the hemp nanopaper. As for the unfilled copolymer, only minor differences were detectable in the thermograms of the composites after crosslinking with UV light. The results are summarized in Figure 8 for the non crosslinked composites along with the thermograms of the pure copolymer and of the nanopaper reported for reference. TGA analyses of crosslinked composites are available in SI (Figure S10).

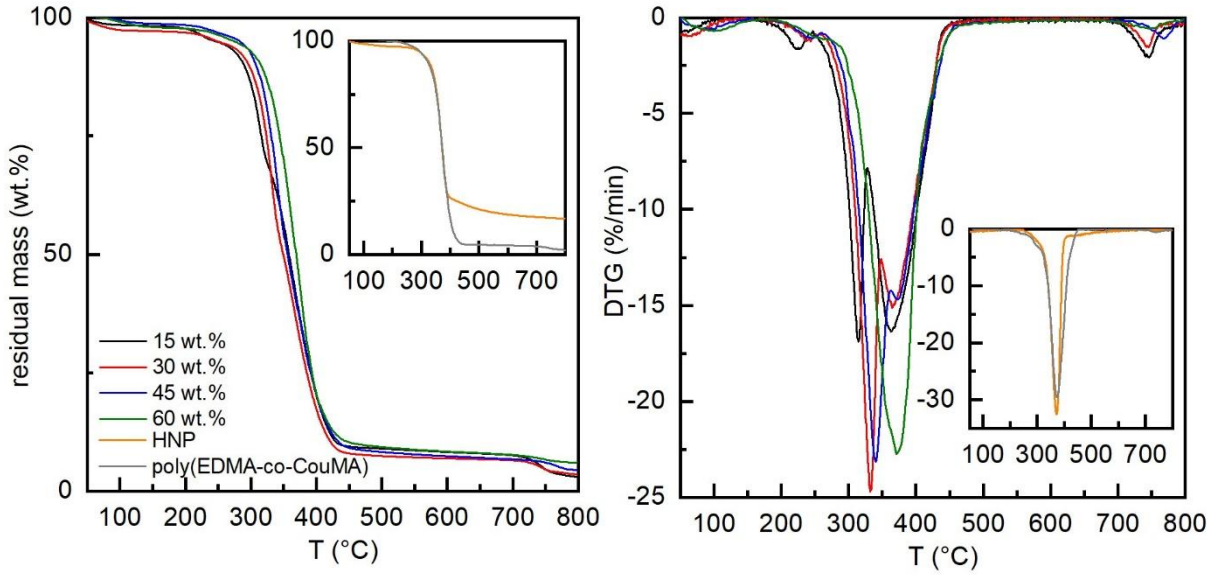

Figure 8 – Thermogravimetric analyses of the composites with 15 wt.% to 60 wt.% of nanocellulose, and of non-filled poly(EDMA-co-CouMA) and hemp nanocellulose handsheet reported as references in the insets: residual mass and first derivative (DTG) of the residual mass curve.

The hemp nanopaper showed only one main weight loss event, at about 360 °C, very close to the T_{max} of the copolymer (373 °C). The composite films on the other hand had more complex weight loss patterns. At low temperatures two small weight losses appeared. The first one around

100 °C may be assigned to the evaporation of residual water, as confirmed by the FTIR spectra of the evolved gas (Figure S3), showing only a broad band above 3300 cm^{-1}, characteristic of O-H stretching. A second small weight loss happened between 225 and 250 °C depending on the cellulose contents, consistent with evaporation of SDS surfactant: only absorptions at 2932 and 2864 cm^{-1} are evidenced in the FTIR analysis of the evolved volatiles. Two distinct mass losses at temperatures above 300 °C were resolved up to 45 wt.% cellulose content. The first main mass loss event was centered at temperatures shifting from 315 °C to 340 °C with cellulose content increasing from 15 wt.% to 45 wt.%: it was attributed to the decomposition of nanocellulose. The second main mass loss remained centered around 370 °C for all composites and was attributed to the decomposition of the copolymer matrix. Indeed, at temperatures corresponding to the first main weight loss, i.e. 300 – 350 °C, the FTIR spectra of the evolved volatile products showed characteristic signals above 3500 cm^{-1} (stretching of O-H), 3100 – 2600 cm^{-1} (stretching of C-H), 2400 – 2200 cm^{-1} (CO_2) , 1800 – 1650 cm^{-1} (carbonyl groups) and 1130 – 1050 cm^{-1} (C-O groups), characteristic of nanocellulose thermal degradation [65], but lacked the signals at 1640, 1609 and 1583 cm^{-1} characteristic of the aromatic and 2-pyrone structures of the copolymer, which were instead visible in the spectra recorded above 380 °C, following the second main mass loss. The two mass loss events eventually overlapped for the 60 wt.% cellulose composite, resulting in one broad peak in the DTG curve centered around 370 °C. The residual masses at 800 °C were not found to increase proportionally to the filler content. A lower thermal stability of nanocellulose at lower weight fractions in composites, as well as lack of proportionality between cellulose content and residue, has also been reported e.g. PVA based composites. This has been attributed to the inability of nanocellulose dispersed in a polymer matrix to form the

tight network of hydrogen-bonded fibrils that imparts high thermal stability to nanocellulose films and promotes carbon formation [66].

CONCLUSIONS

A novel copolymer of ethoxy dihydroeugenyl methacrylate and coumarin methacrylate, was synthesized by redox-initiated radical aqueous emulsion polymerization, obtaining a stable latex. The copolymer was characterized by NMR and FTIR, confirming its structure and composition. The presence of the coumarin moieties allowed the crosslinking of the copolymer, by UV irradiation, exploiting the [2 + 2] photocycloaddition reaction. Being waterborne, the copolymer latex could be easily mixed with an aqueous suspension of hemp nanocellulose: composite films containing up to 85 wt.% biobased content were obtained using an eco-friendly water-based process, suitable for forming self-standing films. The composites were transparent and brownish-colored, with good thermal resistance, although fragile, particularly at low nanocellulose contents. Crosslinking of the composites via photocycloaddition was instrumental in achieving water vapor barrier properties: the WVTR of crosslinked films with up to 45 wt.% of hemp nanocellulose was reduced 5 times with respect to that of nanopaper obtained from the same nanocellulose. It increased approximately ten-fold, when the relative humidity increased from 50% to 90%, to a higher extent for materials containing more cellulose. With their promising barrier properties and good thermal resistance, these materials could be further developed for potential application in packaging as an alternative to current petroleum-based plastics.

ASSOCIATED CONTENT

Supporting Information. The following files are available free of charge.

Supporting Information (PDF): contains Figure S1, Figure S2, Figure S3, Figure S4, Figure S5, Figure S6, Figure S7, Figure S8, Figure S9, Figure S10; Table S1, Table S2, Table S3 and experimental details of colorimetric evaluation.

AUTHOR INFORMATION

Corresponding Author

*sara.dallevacche@polito.it

Author Contributions

The manuscript was written through contributions of all authors. All authors have given approval to the final version of the manuscript.

Funding Sources

ACKNOWLEDGMENTS

The project ComBIOsites has received funding from the European Union's Horizon 2020 research and innovation programme under the Marie Skłodowska-Curie grant agreement No 789454.

Samantha Molina-Gutiérrez thanks the Commission of the European Union for funding her PhD grant through SINCHEM, a Joint Doctorate programme selected under the Erasmus Mundus Action 1 Programme (Framework agreement n° 2013-0037; specific grant agreement n° 532475-EM-5-2017-1-IT-ERAMUNDUS-EPJD).

Giuseppe Ferraro acknowledges funding under the National Recovery and Resilience Plan (NRRP), Mission 4 "Education and Research" - Component 2 "From research to business" -

Investment 3.1 “Fund for the realization of an integrated system of research and innovation infrastructures” - Call for tender No. n. 3264 of 28/12/2021 of Italian Ministry of Research funded by the European Union – NextGenerationEU - Project code: IR0000027, Concession Decree No. 128 of 21/06/2022 adopted by the Italian Ministry of Research, CUP: B33C22000710006, Project title: iENTRANCE.

The authors also thank Loreleï Douard of LGP2 laboratory of the University of Grenoble Alps for assistance in nanocellulose preparation, and Miraç Dizman of Politecnico di Torino for colorimetric measurements. The authors thank Elena Rigo for her assistance during the revision of this paper.

ABBREVIATIONS

TGA thermogravimetric analysis; DSC differential scanning calorimetry; FTIR Fourier transform infrared analysis; ATR attenuated total reflection.

REFERENCES

(1) Kalita, E.; Nath, B. K.; Deb, P.; Agan, F.; Islam, Md. R.; Saikia, K. High Quality Fluorescent Cellulose Nanofibers from Endemic Rice Husk: Isolation and Characterization. *Carbohydr. Polym.* **2015**, *122*, 308–313. https://doi.org/10.1016/j.carbpol.2014.12.075.

(2) Rashid, S.; Dutta, H. Characterization of Nanocellulose Extracted from Short, Medium and Long Grain Rice Husks. *Ind. Crops Prod.* **2020**, *154*, 112627. https://doi.org/10.1016/j.indcrop.2020.112627.

(3) Yang, X.; Han, F.; Xu, C.; Jiang, S.; Huang, L.; Liu, L.; Xia, Z. Effects of Preparation Methods on the Morphology and Properties of Nanocellulose (NC) Extracted from Corn Husk. *Ind. Crops Prod.* **2017**, *109*, 241–247. https://doi.org/10.1016/j.indcrop.2017.08.032.

(4) Hu, L.; Du, H.; Liu, C.; Zhang, Y.; Yu, G.; Zhang, X.; Si, C.; Li, B.; Peng, H. Comparative Evaluation of the Efficient Conversion of Corn Husk Filament and Corn Husk Powder to Valuable Materials via a Sustainable and Clean Biorefinery Process. *ACS Sustain. Chem. Eng.* **2019**, *7* (1), 1327–1336. https://doi.org/10.1021/acssuschemeng.8b05017.

(5) Dai, D.; Fan, M.; Collins, P. Fabrication of Nanocelluloses from Hemp Fibers and Their Application for the Reinforcement of Hemp Fibers. *Ind. Crops Prod.* **2013**, *44*, 192–199. https://doi.org/10.1016/j.indcrop.2012.11.010.

(6) Agate, S.; Tyagi, P.; Naithani, V.; Lucia, L.; Pal, L. Innovating Generation of Nanocellulose from Industrial Hemp by Dual Asymmetric Centrifugation. *ACS Sustain. Chem. Eng.* **2020**, *8* (4), 1850–1858. https://doi.org/10.1021/acssuschemeng.9b05992.
(7) Dalle Vacche, S.; Karunakaran, V.; Patrucco, A.; Zoccola, M.; Douard, L.; Ronchetti, S.; Gallo, M.; Schreier, A.; Leterrier, Y.; Bras, J.; Beneventi, D.; Bongiovanni, R. Valorization of Byproducts of Hemp Multipurpose Crop: Short Non-Aligned Bast Fibers as a Source of Nanocellulose. *Molecules* **2021**, *26* (16), 4723. https://doi.org/10.3390/molecules26164723.
(8) Aulin, C.; Gällstedt, M.; Lindström, T. Oxygen and Oil Barrier Properties of Microfibrillated Cellulose Films and Coatings. *Cellulose* **2010**, *17* (3), 559–574. https://doi.org/10.1007/s10570-009-9393-y.
(9) Poothanari, M. A.; Schreier, A.; Missoum, K.; Bras, J.; Leterrier, Y. Photocured Nanocellulose Composites: Recent Advances. *ACS Sustain. Chem. Eng.* **2022**, *10* (10), 3131–3149. https://doi.org/10.1021/acssuschemeng.1c07631.
(10) Tehfe, M.; Louradour, F.; Lalevée, J.; Fouassier, J.-P. Photopolymerization Reactions: On the Way to a Green and Sustainable Chemistry. *Appl. Sci.* **2013**, *3* (2), 490–514. https://doi.org/10.3390/app3020490.
(11) Bongiovanni, R.; Vacche, S. D.; Vitale, A. Photoinduced Processes as a Way to Sustainable Polymers and Innovation in Polymeric Materials. *Polymers* **2021**, *13* (14), 2293. https://doi.org/10.3390/polym13142293.
(12) Pierau, L.; Elian, C.; Akimoto, J.; Ito, Y.; Caillol, S.; Versace, D.-L. Bio-Sourced Monomers and Cationic Photopolymerization: The Green Combination towards Eco-Friendly and Non-Toxic Materials. *Prog. Polym. Sci.* **2022**, 101517. https://doi.org/10.1016/j.progpolymsci.2022.101517.
(13) Voet, V. S. D.; Guit, J.; Loos, K. Sustainable Photopolymers in 3D Printing: A Review on Biobased, Biodegradable, and Recyclable Alternatives. *Macromol. Rapid Commun.* **2021**, *42* (3), 2000475. https://doi.org/10.1002/marc.202000475.
(14) Lebedevaite, M.; Ostrauskaite, J.; Skliutas, E.; Malinauskas, M. Photoinitiator Free Resins Composed of Plant-Derived Monomers for the Optical μ-3D Printing of Thermosets. *Polymers* **2019**, *11* (1), 116. https://doi.org/10.3390/polym11010116.
(15) Calvino, C. Photocycloadditions for the Design of Reversible Photopolymerizations. *CHIMIA* **2022**, *76* (10), 816–816. https://doi.org/10.2533/chimia.2022.816.
(16) Mariano, M.; El Kissi, N.; Dufresne, A. Cellulose Nanocrystals and Related Nanocomposites: Review of Some Properties and Challenges. *J. Polym. Sci. Part B Polym. Phys.* **2014**, *52* (12), 791–806. https://doi.org/10.1002/polb.23490.
(17) Ansari, F.; Galland, S.; Johansson, M.; Plummer, C. J. G.; Berglund, L. A. Cellulose Nanofiber Network for Moisture Stable, Strong and Ductile Biocomposites and Increased Epoxy Curing Rate. *Compos. Part Appl. Sci. Manuf.* **2014**, *63*, 35–44. https://doi.org/10.1016/j.compositesa.2014.03.017.
(18) Rigo, E.; Ladmiral, V.; Caillol, S.; Lacroix-Desmazes, P. Recent Advances in Radical Polymerization of Bio-Based Monomers in Aqueous Dispersed Media. *RSC Sustain.* **2023**, *1* (4), 788–813. https://doi.org/10.1039/D3SU00097D.
(19) Zhang, L.; Ma, J.; Lyu, B.; Zhang, Y.; Thakur, V. K.; Liu, C. A Sustainable Waterborne Vanillin–Eugenol–Acrylate Miniemulsion with Suitable Antibacterial Properties as a Substitute for the Styrene–Acrylate Emulsion. *Green Chem.* **2021**, *23* (19), 7576–7588. https://doi.org/10.1039/D1GC01766G.

(20) Alexakis, A. E.; Ayyachi, T.; Mousa, M.; Olsén, P.; Malmström, E. 2-Methoxy-4-Vinylphenol as a Biobased Monomer Precursor for Thermoplastics and Thermoset Polymers. *Polymers* **2023**, *15* (9), 2168. https://doi.org/10.3390/polym15092168.
(21) Mahajan, M. S.; Gite, V. V. Self-Healing Polyurethane Coatings of Eugenol-Based Polyol Incorporated with Linseed Oil Encapsulated Cardanol-Formaldehyde Microcapsules: A Sustainable Approach. *Prog. Org. Coat.* **2022**, *162*, 106534. https://doi.org/10.1016/j.porgcoat.2021.106534.
(22) Polunin, Y.; Burns, T. J.; Serum, E. M.; Sibi, M. P.; Voronov, A. Evaluation of 3-Allyl-5-Vinylveratrole in Latex Copolymerization with an Acrylic Monomer from High Oleic Soybean Oil. *ACS Sustain. Chem. Eng.* **2021**, *9* (20), 7003–7011. https://doi.org/10.1021/acssuschemeng.1c00663.
(23) Ladmiral, V.; Jeannin, R.; Fernandes Lizarazu, K.; Lai-Kee-Him, J.; Bron, P.; Lacroix-Desmazes, P.; Caillol, S. Aromatic Biobased Polymer Latex from Cardanol. *Eur. Polym. J.* **2017**, *93*, 785–794. https://doi.org/10.1016/j.eurpolymj.2017.04.003.
(24) Li, W. S. J.; Negrell, C.; Ladmiral, V.; Lai-Kee-Him, J.; Bron, P.; Lacroix-Desmazes, P.; Joly-Duhamel, C.; Caillol, S. Cardanol-Based Polymer Latex by Radical Aqueous Miniemulsion Polymerization. *Polym. Chem.* **2018**, *9* (18), 2468–2477. https://doi.org/10.1039/C8PY00167G.
(25) Molina-Gutiérrez, S.; Li, W. S. J.; Perrin, R.; Ladmiral, V.; Bongiovanni, R.; Caillol, S.; Lacroix-Desmazes, P. Radical Aqueous Emulsion Copolymerization of Eugenol-Derived Monomers for Adhesive Applications. *Biomacromolecules* **2020**, *21* (11), 4514–4521. https://doi.org/10.1021/acs.biomac.0c00461.
(26) Sarker, S. D.; Nahar, L. Progress in the Chemistry of Naturally Occurring Coumarins. In *Progress in the Chemistry of Organic Natural Products 106*; Kinghorn, A. D., Falk, H., Gibbons, S., Kobayashi, J., Eds.; Progress in the Chemistry of Organic Natural Products; Springer International Publishing: Cham, 2017; pp 241–304. https://doi.org/10.1007/978-3-319-59542-9_3.
(27) Ciamician, G.; Silber, P. Chemische Lichtwirkungen. *Berichte Dtsch. Chem. Ges.* **1902**, *35* (4), 4128–4131. https://doi.org/10.1002/cber.19020350450.
(28) Cazin, I.; Rossegger, E.; Guedes de la Cruz, G.; Griesser, T.; Schlögl, S. Recent Advances in Functional Polymers Containing Coumarin Chromophores. *Polymers* **2021**, *13* (1), 56. https://doi.org/10.3390/polym13010056.
(29) Liu, X.; Yi, C.; Zhu, Y.; Yang, Y.; Jiang, J.; Cui, Z.; Jiang, M. Pickering Emulsions Stabilized by Self-Assembled Colloidal Particles of Copolymers of P(St-Alt-MAn)-Co-P(VM-Alt-MAn). *J. Colloid Interface Sci.* **2010**, *351* (2), 315–322. https://doi.org/10.1016/j.jcis.2010.04.056.
(30) Abdollahi, A.; Roghani-Mamaqani, H.; Herizchi, A.; Alidaei-Sharif, H.; Enayati, A.; Sajedi-Amin, S. Light-Induced Spherical to Dumbbell-like Morphology Transition of Coumarin-Functionalized Latex Nanoparticles by a [2π + 2π] Cycloaddition Reaction: A Fast and Facile Strategy to Anisotropic Geometry. *Polym. Chem.* **2020**, *11* (12), 2053–2069. https://doi.org/10.1039/D0PY00078G.
(31) Li, H.; Zhou, J.; Zhao, J. Fabrication of Dual-Functional Cellulose Nanocrystals/Fluorinated Polyacrylate Containing Coumarin Derivatives by RAFT-Assisted Pickering Emulsion Polymerization for Self-Healing Application. *Appl. Surf. Sci.* **2023**, *614*, 156180. https://doi.org/10.1016/j.apsusc.2022.156180.

(32) Zhou, J.; Liu, X.; Wang, X. Photo-Responsive Cellulose Nanocrystal Modified Fluorinated Polyacrylate Based on Coumarin Chemistry. *J. Appl. Polym. Sci.* **2023**, *140* (16), e53757. https://doi.org/10.1002/app.53757.
(33) Zhou, J.; Wang, X.; Liu, X.; Li, X. Design and Synthesis of Waterborne Light-Responsive Cellulose Nanocrystal/Fluorinated Polyacrylate Films toward Oil/Water Repellent and Self-Healing Properties. *Cellulose* **2022**, *29* (14), 7703–7720. https://doi.org/10.1007/s10570-022-04731-2.
(34) Wong, C. S.; Hassan, N. I.; Su'ait, M. S.; Pelach Serra, M. A.; Mendez Gonzalez, J. A.; Granda, L. A.; Badri, K. H. Photo-Activated Self-Healing Bio-Based Polyurethanes. *Ind. Crops Prod.* **2019**, *140*, 111613. https://doi.org/10.1016/j.indcrop.2019.111613.
(35) Qiu, Y.; Munna, D.-R.; Wang, F.; Xi, J.; Wang, Z.; Wu, D. Regulating Asynchronous Deformations of Biopolyester Elastomers via Photoprogramming and Strain-Induced Crystallization. *Macromolecules* **2021**, *54* (12), 5694–5704. https://doi.org/10.1021/acs.macromol.1c00758.
(36) Dalle Vacche, S.; Molina-Gutierrez, Samantha; Ladmiral, Vincent; Caillol, Sylvain; Lacroix-Desmazes, Patrick; Bongiovanni, Roberta. Photochemical [2+2] Cycloaddition of Biobased Latexes for Composites with Microfibrillated Cellulose. *Chem. Eng. Trans.* **2022**, *92*, 277–282. https://doi.org/10.3303/CET2292047.
(37) Molina- Gutiérrez, S.; Manseri, A.; Ladmiral, V.; Bongiovanni, R.; Caillol, S.; Lacroix- Desmazes, P. Eugenol: A Promising Building Block for Synthesis of Radically Polymerizable Monomers. *Macromol. Chem. Phys.* **2019**, *220* (14), 1900179. https://doi.org/10.1002/macp.201900179.
(38) Molina-Gutiérrez, S.; Ladmiral, V.; Bongiovanni, R.; Caillol, S.; Lacroix-Desmazes, P. Emulsion Polymerization of Dihydroeugenol-, Eugenol-, and Isoeugenol-Derived Methacrylates. *Ind. Eng. Chem. Res.* **2019**, *58* (46), 21155–21164. https://doi.org/10.1021/acs.iecr.9b02338.
(39) *Dymax 2000-PC and 5000-PC UV Light Curing Flood Systems*. https://www.uvpacific.com.au/wp-content/uploads/2013/09/lit206eu_2000_pc_5000_pc_uv_curing_flood_lamps_sg.pdf (accessed 2024-04-15).
(40) *LIGHTNINGCURE Spot light source LC8 Hamamatsu Photonics Datasheet*. https://www.hamamatsu.com/content/dam/hamamatsu-photonics/sites/documents/99_SALES_LIBRARY/etd/LC8_TLSZ1008E.pdf (accessed 2024-04-11).
(41) Morales-Cerrada, R.; Molina-Gutierrez, S.; Lacroix-Desmazes, P.; Caillol, S. Eugenol, a Promising Building Block for Biobased Polymers with Cutting-Edge Properties. *Biomacromolecules* **2021**, *22* (9), 3625–3648. https://doi.org/10.1021/acs.biomac.1c00837.
(42) Vitale, D. L.; Icardi, A.; Rosales, P.; Spinelli, F. M.; Sevic, I.; Alaniz, L. D. Targeting the Tumor Extracellular Matrix by the Natural Molecule 4-Methylumbelliferone: A Complementary and Alternative Cancer Therapeutic Strategy. *Front. Oncol.* **2021**, *11*. https://doi.org/10.3389/fonc.2021.710061.
(43) Kuş, N.; Breda, S.; Reva, I.; Tasal, E.; Ogretir, C.; Fausto, R. FTIR Spectroscopic and Theoretical Study of the Photochemistry of Matrix-Isolated Coumarin. *Photochem. Photobiol.* **2007**, *83* (5), 1237–1253. https://doi.org/10.1111/j.1751-1097.2007.00152.x.
(44) Fu, Q.; Cheng, L.; Zhang, Y.; Shi, W. Preparation and Reversible Photo-Crosslinking/Photo-Cleavage Behavior of 4-Methylcoumarin Functionalized

Hyperbranched Polyester. *Polymer* **2008**, *49* (23), 4981–4988. https://doi.org/10.1016/j.polymer.2008.09.017.
(45) Seoane-Rivero, R.; Ruiz-Bilbao, E.; Navarro, R.; Laza, J. M.; Cuevas, J. M.; Artetxe, B.; Gutiérrez-Zorrilla, J. M.; Vilas-Vilela, J. L.; Marcos-Fernandez, Á. Structural Characterization of Mono and Dihydroxylated Umbelliferone Derivatives. *Molecules* **2020**, *25* (15), 3497. https://doi.org/10.3390/molecules25153497.
(46) Trenor, S. R.; Long, T. E.; Love, B. J. Development of a Light-Deactivatable PSA Via Photodimerization. *J. Adhes.* **2005**, *81* (2), 213–229. https://doi.org/10.1080/00218460590922011.
(47) Shanti, R.; N. Hadi, A.; S. Salim, Y.; Y. Chee, S.; Ramesh, S.; Ramesh, K. Degradation of Ultra-High Molecular Weight Poly(Methyl Methacrylate- Co -Butyl Acrylate- Co -Acrylic Acid) under Ultra Violet Irradiation. *RSC Adv.* **2017**, *7* (1), 112–120. https://doi.org/10.1039/C6RA25313J.
(48) Wang, H.-J.; Zhang, H.-Y.; Xing, W.-W.; Wu, H.; Cui, Y.-L.; Liu, Y. Photodimerization-Induced Transition of Helixes to Vesicles Based on Coumarin-12-Crown-4. *Chin. Chem. Lett.* **2022**, *33* (8), 4033–4036. https://doi.org/10.1016/j.cclet.2021.12.051.
(49) Anet, R. The Photodimers of Coumarin and Related Compounds. *Can. J. Chem.* **1962**, *40* (7), 1249–1257. https://doi.org/10.1139/v62-193.
(50) Shi, D.; Matsusaki, M.; Kaneko, T.; Akashi, M. Photo-Cross-Linking and Cleavage Induced Reversible Size Change of Bio-Based Nanoparticles. *Macromolecules* **2008**, *41* (21), 8167–8172. https://doi.org/10.1021/ma800648e.
(51) Abdallh, M.; Hearn, M. T. W.; Simon, G. P.; Saito, K. Light Triggered Self-Healing of Polyacrylate Polymers Crosslinked with 7-Methacryloyoxycoumarin Crosslinker. *Polym. Chem.* **2017**, *8* (38), 5875–5883. https://doi.org/10.1039/C7PY01385J.
(52) Rodionova, G.; Lenes, M.; Eriksen, Ø.; Gregersen, Ø. Surface Chemical Modification of Microfibrillated Cellulose: Improvement of Barrier Properties for Packaging Applications. *Cellulose* **2011**, *18* (1), 127–134. https://doi.org/10.1007/s10570-010-9474-y.
(53) Nair, S. S.; Zhu, J.; Deng, Y.; Ragauskas, A. J. High Performance Green Barriers Based on Nanocellulose. *Sustain. Chem. Process.* **2014**, *2* (1), 23. https://doi.org/10.1186/s40508-014-0023-0.
(54) Solhi, L.; Guccini, V.; Heise, K.; Solala, I.; Niinivaara, E.; Xu, W.; Mihhels, K.; Kröger, M.; Meng, Z.; Wohlert, J.; Tao, H.; Cranston, E. D.; Kontturi, E. Understanding Nanocellulose–Water Interactions: Turning a Detriment into an Asset. *Chem. Rev.* **2023**, *123* (5), 1925–2015. https://doi.org/10.1021/acs.chemrev.2c00611.
(55) Song, Z.; Xiao, H.; Zhao, Y. Hydrophobic-Modified Nano-Cellulose Fiber/PLA Biodegradable Composites for Lowering Water Vapor Transmission Rate (WVTR) of Paper. *Carbohydr. Polym.* **2014**, *111*, 442–448. https://doi.org/10.1016/j.carbpol.2014.04.049.
(56) Lu, P.; Xiao, H.; Pan, Y. Improving Water Vapor Barrier of Green-Based Nanocellulose Film via Hydrophobic Coating. In *Materials Science and Energy Engineering (CMSEE 2014)*; WORLD SCIENTIFIC, 2015; pp 148–153. https://doi.org/10.1142/9789814678971_0023.
(57) Fernández-Santos, J.; Valls, C.; Cusola, O.; Roncero, M. B. Improving Filmogenic and Barrier Properties of Nanocellulose Films by Addition of Biodegradable Plasticizers. *ACS Sustain. Chem. Eng.* **2021**, *9* (29), 9647–9660. https://doi.org/10.1021/acssuschemeng.0c09109.

(58) Spence, K. L.; Venditti, R. A.; Rojas, O. J.; Pawlak, J. J.; Hubbe, M. A. WATER VAPOR BARRIER PROPERTIES OF COATED AND FILLED MICROFIBRILLATED CELLULOSE COMPOSITE FILMS. *BioResources* **2011**, *6* (4), 4370–4388.
(59) Amior, A.; Satha, H.; Vitale, A.; Bongiovanni, R.; Dalle Vacche, S. Photocured Composite Films with Microfibrillated Cellulose: A Study of Water Vapor Permeability. *Coatings* **2023**, *13* (2), 297. https://doi.org/10.3390/coatings13020297.
(60) Duan, Z.; Thomas, N. L. Water Vapour Permeability of Poly(Lactic Acid): Crystallinity and the Tortuous Path Model. *J. Appl. Phys.* **2014**, *115* (6), 064903. https://doi.org/10.1063/1.4865168.
(61) Shogren, R. Water Vapor Permeability of Biodegradable Polymers. *J. Environ. Polym. Degrad.* **1997**, *5* (2), 91–95. https://doi.org/10.1007/BF02763592.
(62) Zhu, H.; Narakathu, B. B.; Fang, Z.; Aijazi, A. T.; Joyce, M.; Atashbar, M.; Hu, L. A Gravure Printed Antenna on Shape-Stable Transparent Nanopaper. *Nanoscale* **2014**, *6* (15), 9110–9115. https://doi.org/10.1039/C4NR02036G.
(63) Scheuing, D. R.; Weers, J. G. A Fourier Transform Infrared Spectroscopic Study of Dodecyltrimethylammonium Chloride/Sodium Dodecyl Sulfate Surfactant Mixtures. *Langmuir* **1990**, *6* (3), 665–671. https://doi.org/10.1021/la00093a023.
(64) Hafizah, M. A. E.; Riyadi, A. F.; Manaf, A.; Andreas. Particle Size Reduction of Polyaniline Assisted by Anionic Emulsifier of Sodium Dodecyl Sulphate (SDS) Through Emulsion Polymerization. *IOP Conf. Ser. Mater. Sci. Eng.* **2019**, *515* (1), 012080. https://doi.org/10.1088/1757-899X/515/1/012080.
(65) Quiévy, N.; Jacquet, N.; Sclavons, M.; Deroanne, C.; Paquot, M.; Devaux, J. Influence of Homogenization and Drying on the Thermal Stability of Microfibrillated Cellulose. *Polym. Degrad. Stab.* **2010**, *95* (3), 306–314. https://doi.org/10.1016/j.polymdegradstab.2009.11.020.
(66) Rowe, A. A.; Tajvidi, M.; Gardner, D. J. Thermal Stability of Cellulose Nanomaterials and Their Composites with Polyvinyl Alcohol (PVA). *J. Therm. Anal. Calorim.* **2016**, *126* (3), 1371–1386. https://doi.org/10.1007/s10973-016-5791-1.